RSC Advances

PAPER

View Article Online
View Journal | View Issue

Cite this: *RSC Adv.*, 2022, **12**, 26418

A new family of NaTMGe (TM = 3d transition metals) half-Heusler compounds: the role of TM modification†

Tuan V. Vu, [ab] Duy Khanh Nguyen,[c] J. Guerrero-Sanchez,[d] J. F. Rivas-Silva,[e] Gregorio H. Cocoletzi[e] and D. M. Hoat *[fg]

Exploring Heusler based materials for different practical applications has drawn more and more attention. In this work, the structural, electronic, magnetic, and mechanical properties of NaTMGe (TM = all 3d transition metals) half-Heusler compounds have been systematically investigated using first-principles calculations. The TM modification plays a determinant role in the fundamental properties. Except NaNiGe and NaCuGe, the studied materials exhibit good dynamical stability. Calculations reveal the non-magnetic semiconductor of NaScGe with a direct energy gap of 1.21 eV. Prospective spintronic applications of NaVGe and NaCrGe–NaMnGe are also suggested by their magnetic semiconductor and half-metallic behavior, respectively, where their magnetic properties follow the Slater–Pauling rule. Nevertheless, the remaining materials are either magnetic or non-magnetic metallic. For the magnetic systems, the magnetism is induced mainly by the TM constituents with either spin-up (V, Cr, Mn, and Fe) or spin-down (Co) 3d states. Calculated elastic constants indicate that all compounds are mechanically stable. Furthermore, they exhibit significant elastic anisotropy, where NaScGe and NaZnGe are the least and most anisotropic materials, respectively. Also, modifying the TM elements influences the materials' ductile and brittle behaviors. Our work unravels clearly the effects of TM modification on the fundamental properties of NaTMGe compounds. NaTMGe materials show excellent versatility with promising properties for optoelectronic and spintronic applications.

Received 11th May 2022
Accepted 21st August 2022

DOI: 10.1039/d2ra02983a

rsc.li/rsc-advances

1 Introduction

Manipulating electron spins has led to the discovery of new physics and the emergence of novel properties. Spin current in ferromagnetic (FM) Fe, Co, Ni, and Gd films has been observed by Tedrow *et al.*[1] Experimental observation of the tunnel magneto-resistance (TMR) effect has been realized by Julliere *et al.*,[2] where electrons can tunnel from an Fe ferromagnet to a Co ferromagnet in an Fe–Ge–Co film junction. Later, Fert *et al.*[3] discovered the giant magnetoresistance effect in (001)Fe/(001)Cr magnetic superlattices, for which the authors were awarded the Nobel Prize in Physics. These works and others have stimulated the emergence of spin-based electronics, also known as spintronics. Spintronics is a discipline that has appeared to revolutionize information technology. As an additional degree of freedom, handling electron spins allows controlling the electrical current in the presence of any external magnetic field.[4] In general, spintronics technology function follows a basic principle: (1) the information is stored in electron spins; (2) the information is transported through electron spins; and (3) the information is read at the final terminal. In comparison with conventional electronics based on electron charge, spintronics exhibits some advantages such as massive information storage, high-speed processing, and low energy consumption,[5] which point to spintronics as a promising alternative to existing information technology. In the last few years, the applications of spintronics have been continuously increasing and its

[a]*Laboratory for Computational Physics, Institute for Computational Science and Artificial Intelligence, Van Lang University, Ho Chi Minh City, Vietnam. E-mail: tuan.vu@vlu.edu.vn*

[b]*Faculty of Mechanical - Electrical and Computer Engineering, Van Lang University, Ho Chi Minh City, Vietnam*

[c]*High-Performance Computing Lab (HPC Lab), Information Technology Center, Thu Dau Mot University, Binh Duong Province, Vietnam. E-mail: khanhnd@tdmu.edu.vn*

[d]*Universidad Nacional Autónoma de México, Centro de Nanociencias y Nanotecnología, Apartado Postal 14, Ensenada, Baja California, Código Postal 22800, Mexico*

[e]*Benemérita Universidad Autónoma de Puebla, Instituto de Física, Apartado Postal J-48, Puebla 72570, Mexico. E-mail:*

[f]*Institute of Theoretical and Applied Research, Duy Tan University, Ha Noi 100000, Vietnam. E-mail: dominhhoat@duytan.edu.vn*

[g]*Faculty of Natural Sciences, Duy Tan University, Da Nang 550000, Vietnam*

† Electronic supplementary information (ESI) available. See https://doi.org/10.1039/d2ra02983a

extension in industry has been estimated to reach a rate beyond Moore's law.[6] In spintronic devices, the generation of spin-polarized electrons plays a key role. So far, two methods have been widely employed:

• Spin injection from highly spin-polarized materials such as FM metals, or half-metallic or diluted magnetic semiconductors.[7–9]

• Spin filtering that makes use of the spin-dependent barrier height. In this case, magnetic semiconductor materials are desirable due to the different potential felt by electron spins.[10,11]

Speaking about spintronic materials, it would be wrong not to mention Heusler compounds that have formed one of the most exciting materials classes. Going back to history, the ferromagnetism has been found in ternary Cu_2MnAl despite none of its constituent elements being ferromagnetic in nature.[12] Until today, an endless collection of Heusler compounds has been explored by combining different possible elements of the periodic table. In terms of composition, they can be categorized into the following sub-groups: (1) full-Heusler X_2YZ (stoichiometry 2 : 1 : 1); (2) half-Heusler XYZ (stoichiometry 1 : 1 : 1); and (3) equiatomic quaternary Heusler XX′YZ (stoichiometry 1 : 1 : 1 : 1), where Z is a main group element.[13–18] Containing transition metals as constituents, many Heusler compounds exhibit feature-rich electronic and magnetic properties. In 1983, Groot *et al.*[19] predicted half-metallicity in the NiMnSb alloy using first-principles calculations. The results show a metallic spin-up channel and a semiconductor spin-down channel, giving rise to a spin-polarization of 100%. In the same year, the density of states of the Co_2MnAl and Co_2MnSn ternary compounds calculated by Kübler *et al.*[20] revealed that the spin-down channel vanishes at the Fermi energy, which induces a high spin-polarization. These predictions have drawn special attention towards ferromagnetic Heusler alloys, such that incessant investigations have been carried out to provide deeper and deeper insight into these materials. In general, the total magnetic moments μ in Heusler alloys can be predicted using the Slater–Pauling rule:[21] $\mu = N_v - 24$ or $\mu = N_v - 18$, where N_v is the total number of valence electrons. Besides half-metallicity,[22,23] spin-gapless semiconductor and magnetic semiconductor natures[24–27] have also been observed, and are suitable for spintronic applications.

Half-Heusler compounds have been considered as promising electrode materials for giant magnetoresistance and spin injection applications.[28–31] Theoretically, researchers have explored a large variety of half-Heusler compounds using first-principles calculations. For examples, despite containing transition metals as constituents, RuVX (X = As, P, and Sb) compounds exhibit non-magnetic semiconductor nature with band gaps between 0.49 and 0.59 eV.[32] Feature-rich half-metallicity has been found in XCrZ (X = Li, K, Rb, Cs; Z = S, Se, Te),[33] RhFeZ (X = Ge and Sn),[34,35] and CrXPb (X = Sc and Ti).[36] Interestingly, Umamaheswari *et al.*[37] have demonstrated half-metallic ferromagnetism in half-Heusler compounds containing neither transition metals nor rare earths XYZ (X = Li, Na, K and Rb; Y = Mg, Ca, Sr and Ba; Z = B, Al and Ga), which is generated mainly by s and p electrons. Undoubtedly, the fundamental properties of half-Heusler compounds vary depending on their chemical composition.[38,39] Previously, the semiconducting NaScGe compound was investigated by Ciftci *et al.*[40] and Kacimi *et al.*[41] However, as far as we are aware, the structural, electronic, magnetic, and elastic properties of most of the NaTMGe (TM = all 3d transition metals) compounds have not been investigated well. In this work, our main aim is to investigate systematically these new half-Heusler compounds. From the obtained results, we will be able to recommend new candidates for possible optoelectronic and spintronic applications.

2 Computational details

To investigate NaTMGe half-Heusler compounds, density functional theory (DFT)[42] as incorporated in the WIEN2k package[43] has been used, which makes use of the full-potential linearized augmented plane wave (FP-LAPW) basis set. In this method, the wave functions are differently expanded in two regions: (1) inside atomic spheres (muffin-tin), the basis set expansion is realized using atomic orbitals and (2) in the interstitial region, plane wave functions are employed. These are interconnected through continuity and differentiability conditions. During calculations, the cut-off energies of $l_{max} = 10$ and the product of $R_{MT} \times K_{max} = 8$ are set for expansion in the first and second regions, respectively. Herein, l_{max} is the maximum quantum number of spherical harmonics. R_{MT} and K_{max} are the smallest muffin-tin radius and largest wave vector, respectively. A Monkhorst–Pack k-grid[44] of 20 × 20 × 20 is generated to sample the Brillouin zone. The self-consistency convergence is set to 10^{-5} Ryd for the energy difference between two consecutive iterations. The Perdew–Burke–Ernzerhof based-Generalized Gradient Approximation (PBE-GGA)[45] is adopted for the treatment of exchange–correlation potentials. In order to achieve a more accurate band gap calculation and better treatment of highly correlated electrons (3d), the modified Becke–Johnson (mBJ) potential is also employed.[46–48] In addition, the elastic constants have been calculated using the stress–strain method from the second derivative of the fitted energy–strain polynomial:[49,50]

$$E(\varepsilon) = E(0) + \sum_{i=1}^{6} \frac{\partial E}{\partial \varepsilon_i}\varepsilon_i + \frac{1}{2}\sum_{i,j=1}^{6} \frac{\partial^2 E}{\partial \varepsilon_i \partial \varepsilon_j}\varepsilon_i \varepsilon_j \quad (1)$$

$$C_{i,j} = \frac{1}{V_0}\frac{\partial^2 E}{\partial \varepsilon_i \partial \varepsilon_j} \quad (2)$$

3 Results and discussion

3.1 Structural properties

The half-Heusler NaTMGe compounds crystallize in a cubic structure belonging to the $F\bar{4}3m$ space group (no. 216). Fig. 1 shows three possible configurations of the constituent atoms. In the type-I structure, Na, TM, and Ge atoms occupy the 4a (0; 0; 0), 4c (0.25; 0.25; 0.25), and 4d (0.75; 0.75; 0.75) Wyckoff

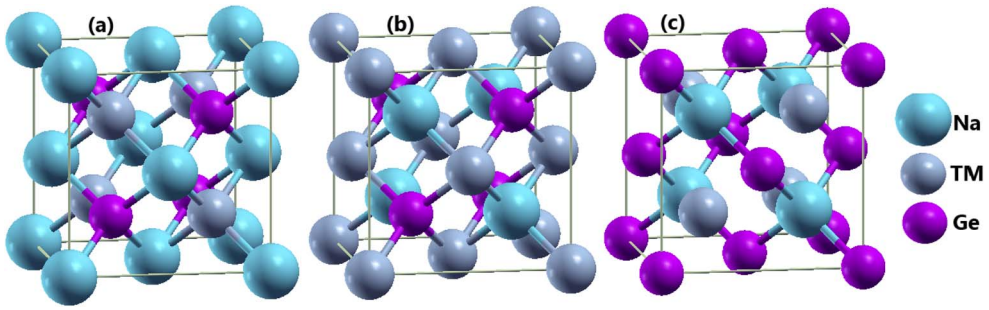

Fig. 1 (a) I-type, (b) II-type, and (c) III-type crystal structures of NaTMGe half-Heusler compounds.

positions, respectively. In the type-II structure, they are situated at the 4c, 4a, and 4d positions, respectively. In the type-III structure, Na and TM atoms occupy the 4c and 4d positions, respectively, while Ge atoms are located at the 4a position.[51] There are four unit formulae in each unit cell. As a first step, the total energy is calculated at different cell volumes considering both non-magnetic (NM) and ferromagnetic (FM) states to determine the stable structure. It is worth mentioning that most Heusler-based alloys are FM materials,[52–57] therefore only NM and FM phases are considered herein. Calculated energies as a function of primitive cell are plotted in Fig. 2. In all structures, NaScGe, NaTiGe, NaCoGe, NaNiGe, NaCuGe, and NaZnGe compounds exhibit negligible difference in energy between FM and NM states. In contrast, the FM phase appears to be stable in the remaining materials due to its smaller energy. Furthermore, the calculated energies also reveal that the type-III structure is energetically favorable for the compounds with TM elements from Sc to Mn. In contrast, element modification with the last five members of the 3d TM row causes the considered materials to crystallize in the type-II structure.

Once the stable magneto-structural phase has been determined, the geometry is optimized using an energy–volume (E–V) Birch–Murnaghan equation of state as follows:[58]

$$E(\mathrm{V}) = E_0 + \frac{9V_0B}{16}\left\{\left[\left(\frac{V_0}{V}\right)^{2/3} - 1\right]^3 B' + \left[\left(\frac{V_0}{V}\right)^{2/3} - 1\right]^2\left[6 - 4\left(\frac{V_0}{V}\right)^{2/3}\right]\right\} \quad (3)$$

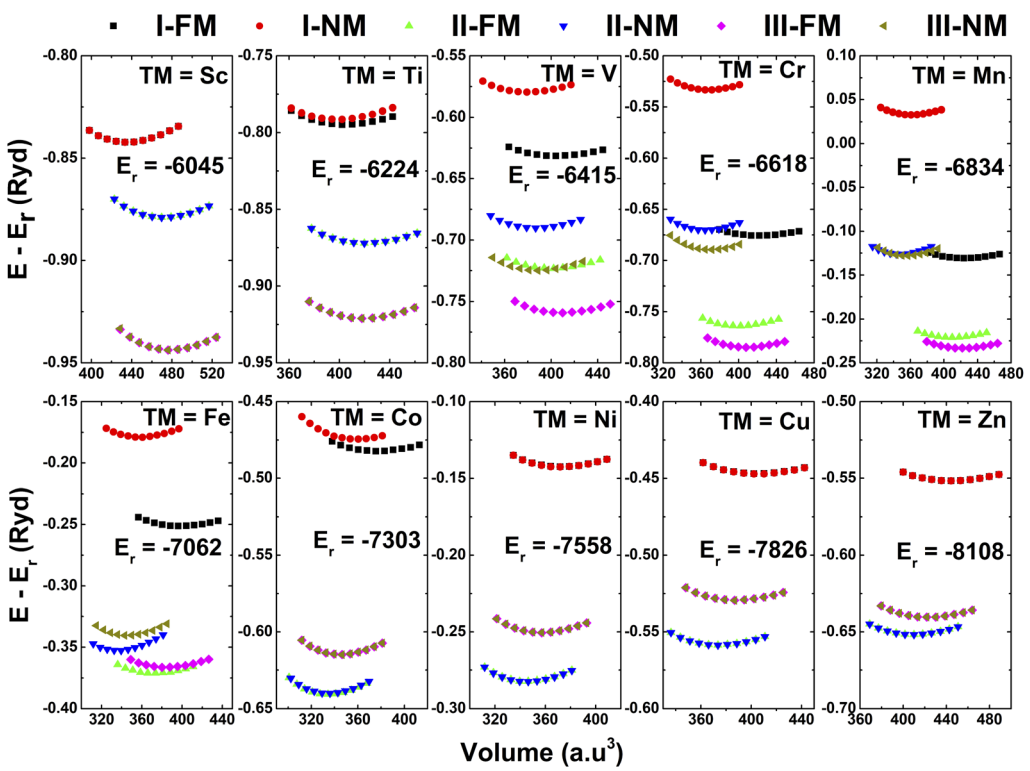

Fig. 2 Calculated energy of NaTMGe half-Heusler compounds as a function of volume (FM = ferromagnetic; NM = non-magnetic).

Table 1 Lattice constant a (Å), formation enthalpy ΔH_f (eV per atom), spin-up/spin-down band gap E_g (eV) (M = metal), spin polarization P (%), and magnetic moments μ (T: total; I: interstitial) (μ_B) of NaTMGe half-Heusler compounds

					μ			
	a	ΔH_f	E_g	P	T	I	Na	TM	Ge
TM = Sc	6.57	−2.42	1.21/1.21						
TM = Ti	6.29	−1.92	M/M						
TM = V	6.24	−1.63	0.12/1.12		2.00	0.10	−0.01	2.07	−0.15
TM = Cr	6.23	−1.62	M/1.70	100	3.00	0.02	−0.04	3.52	−0.50
TM = Mn	6.30	−1.98	M/1.53	100	4.00	0.14	−0.01	4.21	−0.34
TM = Fe	6.05	−1.60	M/M	40.24	3.03	0.10	0.02	3.02	−0.10
TM = Co	5.83	−1.71	M/M	15.79	−0.41	0.02	−0.01	−0.48	0.05
TM = Ni	5.89	−1.91	M/M						
TM = Cu	6.05	−1.92	M/M						
TM = Zn	6.24	−2.09	M/M						

After fitting the E–V data to eqn (3), the minimization procedure is employed to calculate the equilibrium lattice constant. The obtained results are listed in Table 1. Note that this structural parameter varies according to the 3d TM element, where the NaScGe and NaCoGe compounds exhibit the largest (6.57 Å) and smallest (5.83 Å) values, respectively. Undoubtedly, these results are mainly related to the atomic size of the transition metals.

Theoretically, as a reliable approach, phonon dispersion curves have been widely employed to examine the dynamical stability of materials. The absence of significant negative phonon frequencies may indicate a good dynamical stability, otherwise the material may possess a poor stability.[59] Fig. 3 displays the calculated phonon spectra of NaTMGe half-Heusler compounds. The results indicate that eight compounds, namely NaScGe, NaTiGe, NaVGe, NaCrGe, NaMnGe, NaFeGe, NaCoGe, and NaZnGe, are dynamically stable since their spectra exhibit only positive phonon frequencies. In contrast, significant imaginary phonon modes up to −53.41 (cm^{-1}) and −51.78 (cm^{-1}), respectively, suggest dynamical instability of the NaNiGe and NaCuGe compounds. Despite their poor stability, the electronic, magnetic, and elastic results of these two materials will still be presented in the following subsections for comparisons.

In addition, the thermodynamic stability is analyzed through the formation enthalpy ΔH_f parameter, which is calculated as follows:

$$\Delta H_f = \frac{E(t) - (n_{Na}\mu(Na) + n_{TM}\mu(TM) + n_{Ge}\mu(Ge))}{n_{Na} + n_{TM} + n_{Ge}} \quad (4)$$

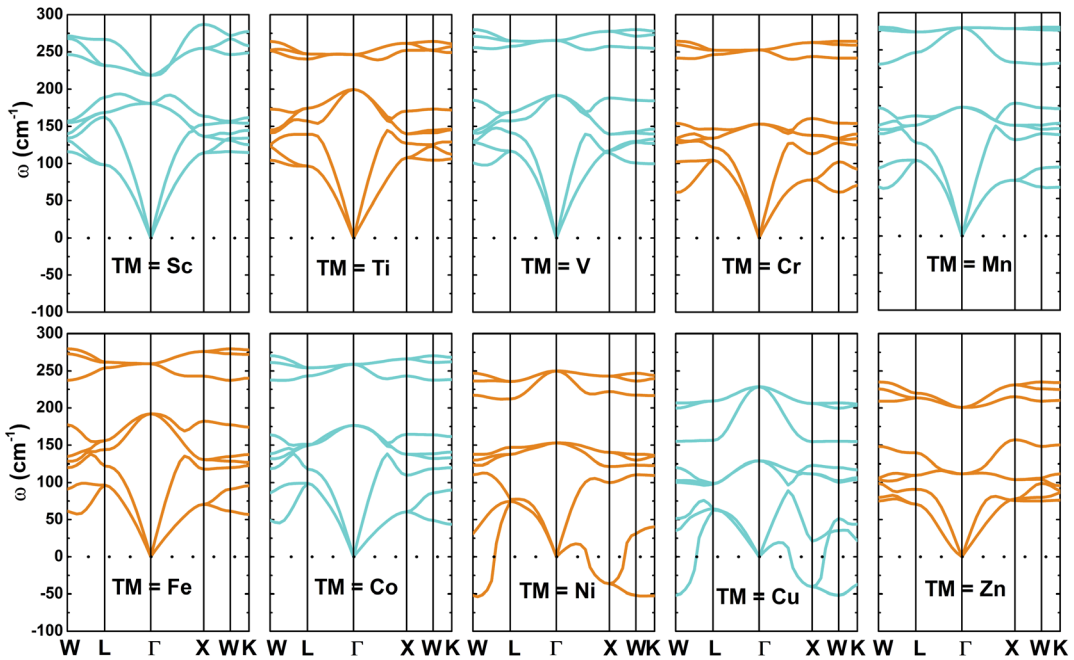

Fig. 3 Phonon dispersion curves of NaTMGe half-Heusler compounds (III-type structure for TM = Sc, Ti, V, Cr, and Mn; II-type structure for TM = Fe, Co, Ni, Cu, and Zn).

where $E(t)$ is the total system energy and μ denotes the chemical potential of each element with the corresponding number of atoms n. The results are given in Table 1, and confirm that NaTMGe half-Heusler compounds are thermodynamically stable considering their negative ΔH_f values. Note that NaScGe and NaFeGe are the most and least stable materials as suggested by their most negative and most positive ΔH_f, respectively.

3.2 Electronic properties

The calculated spin-resolved band structures of NaTMGe compounds are displayed in Fig. 4. Simulations reveal non-spin-polarized behavior in the NaScGe, NaTiGe, NaNiGe, NaCuGe, and NaZnGe compounds, suggesting their NM equilibrium properties. The obtained band gaps are given in Table 1. Interestingly, NaScGe is a direct gap semiconductor with an energy gap of 1.21 eV since both the valence band maximum (VBM) and conduction band minimum (CBM) occur at the X point. This value is larger than that obtained in previous calculations (1.02 eV (ref. 40 and 41)), which may be due to the difference in the design of the material's structure. Meanwhile, a significant overlapping of either the conduction band or valence band with the Fermi level indicates the metallic nature of the NaTiGe, NaNiGe, NaCuGe, and NaZnGe compounds. In contrast, the band structures exhibit a clear spin-asymmetry for TMs from V to Co, where the electronic properties vary from one to another. Specifically, the NaVGe compound is a magnetic semiconductor material. Meanwhile, a metallic spin-up state and a semiconductor spin-down state indicate the half-metallic nature of the NaCrGe and NaMnGe compounds (see their band gap values in Table 1). Previously, half-metallicity was also found in NaCrAs and NaCrSb,[60,61] and the spin-dependent energy gaps may vary between the employed constituent main group atoms. In contrast, one can see a significant intersection with the Fermi level for the NaFeGe and NaCoGe electronic states in both of their spin configurations, indicating their magnetic metallic ground state properties. It is worth recalling that the magnetic semiconductor and half-metallic properties suggest the NaVGe and NaCrGe–NaMnGe compounds as prospective materials to create highly spin-polarized electrons through spin filtering and spin injection, respectively.

In order to gain more insight into the band structure formation, the projected densities of states of NaTMGe half-Heusler compounds are calculated, and the results are given in Fig. 5 (see Fig. S1† for NaMnGe, NaCoGe, NaCuGe, and NaZnGe). In the considered energy range from −2 to 4 eV, the band structure originates mainly from Ge-p and TM-d states. Specifically, the upper part of the valence band is formed mainly by Ge-p and TM-$d_{t_{2g}}$ states. The former exhibits higher weight in the spin-down channel than in the spin-up channel of the magnetic systems. Meanwhile, the major contribution to the conduction band comes from the two-fold degenerate TM-3d states. Note that the metallic spin configurations are induced by either TM-$3d_{t_{2g}}$ or Ge-p states since they spread from the upper part of the valence band to the lower part of the conduction band overlapping with the Fermi level.

As mentioned above, high spin-polarization (P) is a criterion to selectively choose materials for spintronic applications. We have calculated the P parameter for some half-Heusler compounds studied in this work using the following formula:[62]

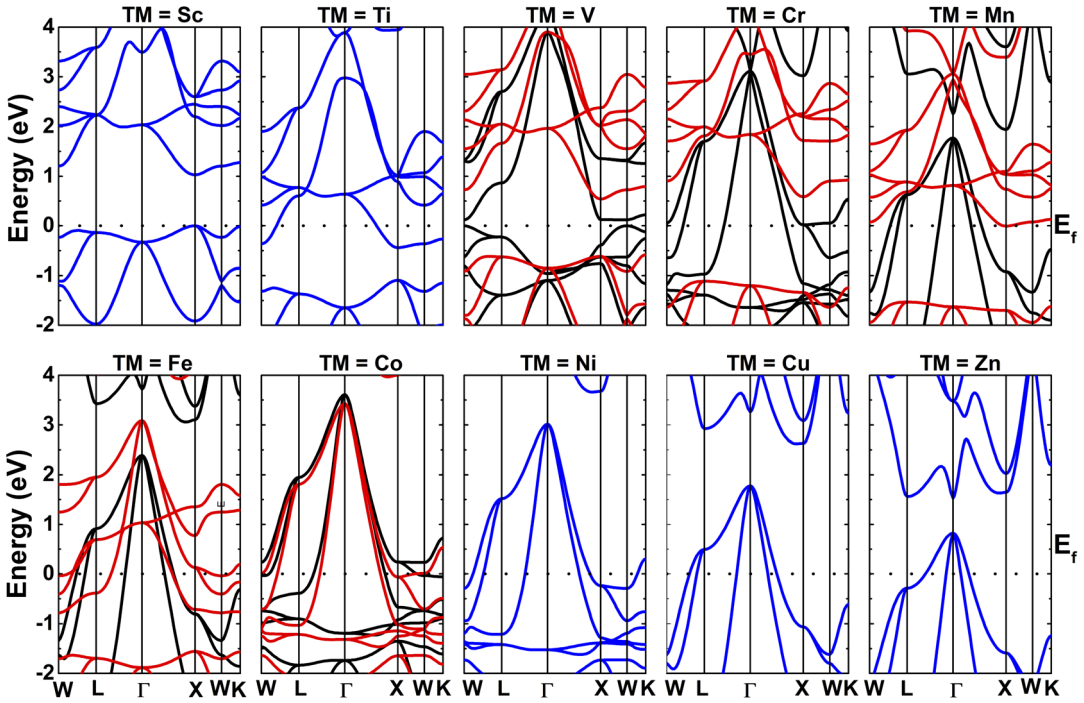

Fig. 4 Electronic band structures of NaTMGe half-Heusler compounds (black line: spin-up; red line: spin-down; blue line: non-spin-polarized).

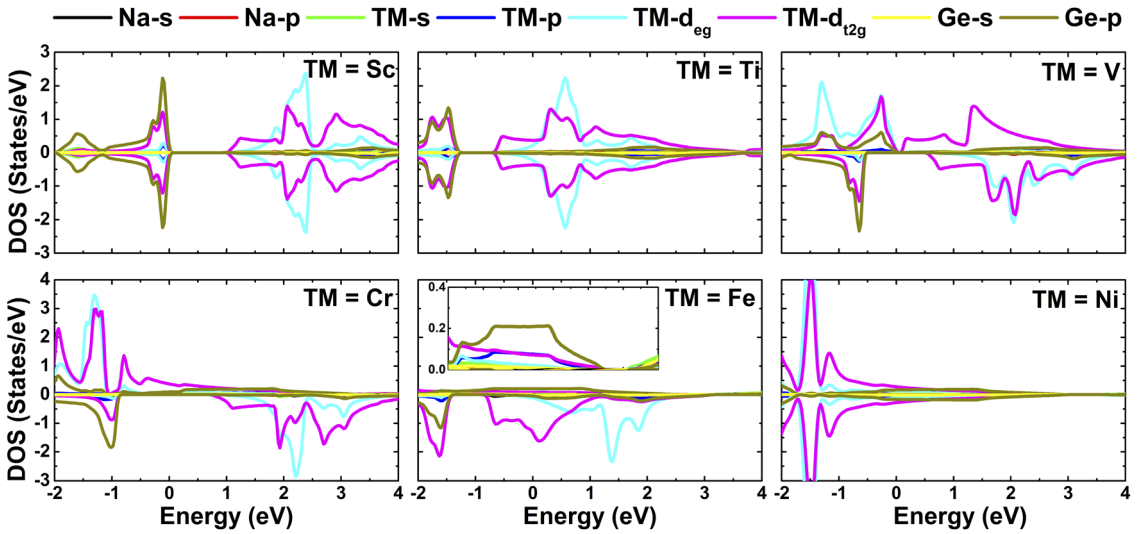

Fig. 5 Projected densities of states of NaTMGe half-Heusler compounds.

$$P = \frac{|N_F(\uparrow) - N_F(\downarrow)|}{N_F(\uparrow) - N_F(\downarrow)} \times 100\% \quad (5)$$

where $N_F(\uparrow)$ and $N_F(\downarrow)$ refer to the density of states values at the Fermi level for spin-up and spin-down states, respectively. The results are given in Table 1. The half-metallic nature provides a perfect spin-polarization of 100% to the NaCrGe and NaMnGe ternary compounds. Meanwhile, P takes quite small values of 40.24% and 15.79% in the cases of NaFeGe and NaCoGe, respectively, which may suggest a poor spintronic performance for these materials.

3.3 Magnetic properties

Spin-asymmetric band structures indicate significant magnetism in the half-Heusler NaTMGe (TM = V, Cr, Mn, Fe, and Co) compounds. To characterize the magnetic properties, their total and local magnetic moments have been calculated, and are listed in Table 1. It is worth mentioning that an integer total magnetic moment is a characteristic of magnetic semiconductor and half-metallic materials.[27,63] This feature is also satisfied for the NaVGe, NaCrGe, and NaMnGe ternary compounds with values of 2.00, 3.00, and 4.00 (μ_B), respectively. Note that these compounds have a total number of 20, 21, and 22 valence electrons, respectively (summing one for Na-3s^1, five for V-3d^{3}4s^2, six for Cr-3d^{5}4s^1, seven for Mn-3d^{5}4s^2, and fourteen for Ge-3d^{10}4s^{2}4p^2). Therefore, their magnetic properties satisfy the Slater–Pauling rule:

$$\mu = N_v - 18 \quad (6)$$

Significant magnetism is also obtained in NaFeGe with a total value of 3.03 (μ_B). In these four mentioned materials, the magnetic properties are produced mainly by the TM spin-up states with positive local magnetic moments of V, Cr, Mn, and Fe of 2.07, 3.52, 4.21, and 3.02 (μ_B), respectively. A small contribution from the spin-down states of Ge atoms can also be noted. In contrast, the magnetization of NaCoGe is induced mainly by the Co spin-down electrons with a local magnetic moment of −0.48 (μ_B), while a small total value of −0.41 (μ_B) indicates its lower magnetism as compared to the above ternary compounds.

Readers can find an illustration of these analyzed results in Fig. S2,† where the spin densities are displayed. From the figures, one can see that TM atoms generate the magnetic properties. In the cases of NaVGe, NaCrGe, NaMnGe, and NaFeGe, the spin-up densities are accumulated at V, Cr, Mn, and Fe sites, respectively. Meanwhile, spin-down density accumulation is observed at the Co site in NaCoGe, where its low magnetism is also suggested by a small iso-surface.

Besides the mBJ potential, the DFT+U approach has been widely applied to investigate magnetic systems containing transition metals because of its effective treatment of highly correlated electrons.[64] Therefore, additional mBJ-GGA+U calculations have been performed to corroborate the electromagnetic properties of the NaVGe, NaCrGe, NaMnGe, and NaFeGe compounds. Herein, a $U_{eff} = U - J$ parameter of 4 eV is applied on the TM-3d orbital, which has been previously employed by many research groups to provide a reasonable description of fundamental properties.[65,66] Readers can find the calculated band structures displayed in Fig. S2,† and energy gaps and magnetic moments listed in Table S1.† Despite a slight difference in the calculated spin-dependent band gaps, the mBJ-GGA+U approach provides quite similar electronic band structure profiles as compared to the mBJ-GGA functional. Specifically, magnetic semiconductor and half-metallic characters are obtained for the NaVGe and NaCr(Mn)Ge compounds, respectively. Consequently, they possess integer total magnetic moments of 2 and 3(4) (μ_B), respectively. Meanwhile, the NaFeGe ternary compound exhibits metallic nature in both of its spin states. The transition metals contribute mainly to the magnetic properties as revealed by their large magnetic moments. It is worth

mentioning that both methods yield quite similar features, confirming their reliability.

3.4 Mechanical properties

In practice, stress and strain are frequent factors applied intentionally or not to materials, and a structural deformation is inevitable. Therefore, when designing materials for practical applications, a systematical study on their ability to return to their original form, once the stress and strain are removed, is very important. This materials feature can be analyzed through elastic constants. Crystallizing in a cubic structure, the elasticity of the materials studied herein is characterized by three elastic constants, namely C_{11}, C_{12}, and C_{44}. Their calculated values are given in Table 2. Born criteria have been established to determine the mechanical stability as follows:[67] $C_{11} > 0$; $C_{44} > 0$, $C_{11} > C_{12}$, and $C_{11} + 2C_{12} > 0$. Note that none of these criteria are violated in the considered NaTMGe half-Heusler compounds, indicating that they are mechanically stable. Moreover, the considerably larger C_{11} values in comparison with the C_{44} values may indicate a higher resistance to longitudinal deformation than to shear deformation for these materials.

From the calculated elastic constants, some mechanical parameters can be derived as follows:[68]

$$B = \frac{C_{11} + 2C_{12}}{3} \tag{7}$$

$$G = \frac{G_V + G_R}{2} \tag{8}$$

where G_V and G_R correspond to the Voigt and Reuss components, respectively:

$$G_V = \frac{C_{11} - C_{12} + 3C_{44}}{5} \tag{9}$$

$$G_R = \frac{5(C_{11} - C_{12})C_{44}}{4C_{44} + 3(C_{11} - C_{12})} \tag{10}$$

$$E = \frac{9BG}{3G + B} \tag{11}$$

$$A = \frac{2C_{44}}{C_{11} - C_{12}} \tag{12}$$

$$\gamma = \frac{3B - 2G}{6B + 2G} \tag{13}$$

where B, G, E, A, and γ are the bulk modulus, shear modulus, Young's modulus, anisotropy, and Poisson ratio, respectively. All determined values are given in Table 2.

Large bulk modulus values are indicators of a good materials resistance to compression. From Table 2, it can be noted that NaCoGe is the hardest material and NaMnGe exhibits the highest compressibility considering their largest and smallest bulk modulus, respectively. Also, the shear modulus is considerably smaller than the bulk modulus, in agreement with the relationship between the C_{11} and C_{44} constants, confirming again a better resistance to uniaxial deformation than to shear deformation. In general, the Young's modulus is employed to examine the materials stiffness. The larger the Young's modulus is, the stiffer the material will be. As shown in Table 2, NaCoGe is the stiffest material, while the softest one is NaMnGe. This result also reveals the poor resistance to stress and strain of the NaMnGe compound.

Elastic anisotropy A is an important parameter to examine the defect distribution and crack formation of materials. A homogeneous distribution of defects and cracks is indicated by elastic isotropy, corresponding to a unity value of A.[69] Any deviation from this value may indicate elastic anisotropy. Note from Table 2 that none of the studied compounds has an A value of 1, indicating that all are elastically anisotropic. The first and last material of the row exhibit the lowest and highest anisotropy, respectively. To illustrate this feature, their dependent directional Young's moduli in both 3D and 2D are displayed in Fig. 6 (see Fig. S4† for the remaining materials), using the ELATE analyzer.[70] Note that the 3D surface of NaScGe is nearly spherical and its projections are nearly circular, suggesting a quite low anisotropy. In contrast, the non-spherical 3D surface and non-circular 2D projections agree well with the strong deviation from unity of the NaZnGe elastic anisotropy parameter.

The Poisson ratio γ and Pugh index (B/G) provide useful insights into the characteristics of materials bonding forces. The critical values of these parameters have been determined to

Table 2 Elastic constants C_{11}, C_{12}, and C_{44} (GPa); bulk modulus B, shear modulus G, and Young's modulus E (GPa); anisotropy A; Poisson ratio γ; and Pugh index B/G of NaTMGe half-Heusler compounds

	C_{11}	C_{12}	C_{44}	B	G	E	A	γ	B/G
TM = Sc	94.28	26.20	32.94	48.89	33.38	98.56	0.97	0.22	1.46
TM = Ti	104.29	39.46	37.88	61.07	35.59	116.55	1.17	0.26	1.72
TM = V	95.57	34.69	18.81	54.98	22.83	91.50	0.62	0.32	2.41
TM = Cr	93.47	23.21	21.88	46.63	26.47	88.14	0.62	0.26	1.76
TM = Mn	53.40	24.39	11.14	34.06	12.38	53.30	0.75	0.34	2.75
TM = Fe	78.61	34.07	20.85	48.92	21.41	83.30	0.94	0.31	2.29
TM = Co	131.93	47.49	37.84	75.64	39.53	138.55	0.90	0.28	1.91
TM = Ni	115.02	44.06	19.20	67.71	24.61	105.96	0.54	0.34	2.75
TM = Cu	81.76	37.97	24.80	52.57	23.40	90.49	1.13	0.30	2.23
TM = Zn	54.71	34.80	27.50	41.44	18.30	70.85	2.76	0.31	2.26

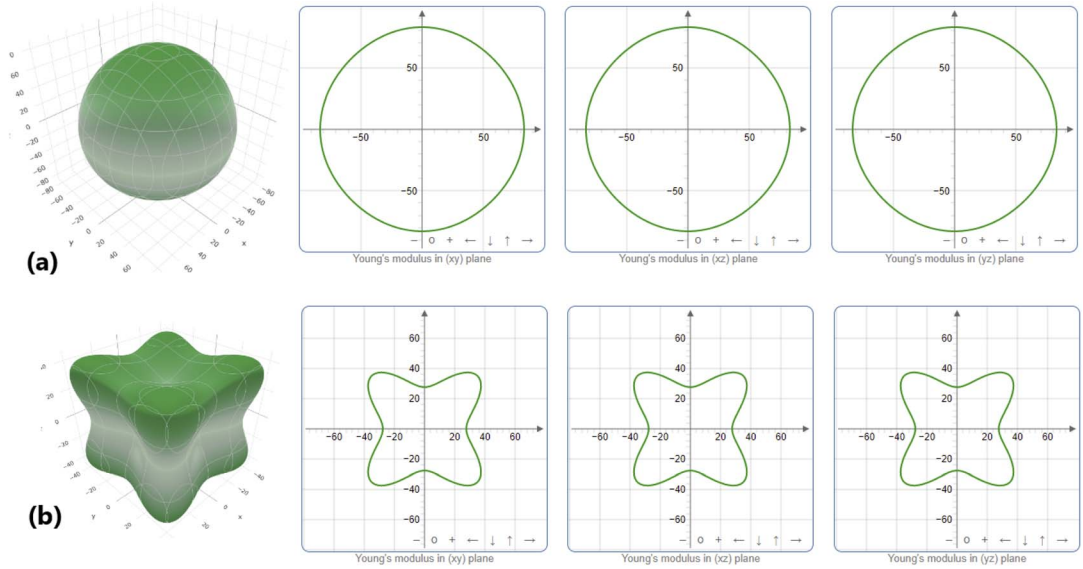

Fig. 6 Directional dependence of the Young's modulus of (a) NaScGe and (b) NaZnGe half-Heusler compounds.

be 0.26 and 1.75,[71] respectively. Larger values indicate a ductile nature, and otherwise the material is mechanically brittle. The values listed in Table 2 suggest brittleness for NaScGe and NaTiGe, whereas the remaining half-Heusler compounds are mechanically ductile. It is worth mentioning that different atomic arrangements may affect the parameters, however our elastic and mechanical properties of NaScGe are in agreement with previous calculations by Ciftci *et al.*[40]

4 Conclusions

In conclusion, a series of first-principles calculations has been performed to investigate the structural, electronic, magnetic, and mechanical properties of NaTMGe (TM = all 3d transition metals) half-Heusler compounds. For the first five members of the TM row, the ternary compounds crystallize in the type-III structure in which Na, TM, and Ge are located at the 4c, 4d, and 4a Wyckoff positions, respectively. Meanwhile, the remaining five compounds prefer to adopt the type-II structure, where their constituent atoms occupy the 4c, 4a, and 4d positions, respectively. Calculated phonon dispersion curves confirm the dynamical stability of the studied compounds, with the exception of NaNiGe and NaCuGe. The results indicate that NaScGe, NaTiGe, NaNiGe, NaCuGe, and NaZnGe are non-magnetic materials, where the first one is a direct gap semiconductor with a relatively large band gap of 1.21 eV. NaVGe is a magnetic semiconductor system, while half-metallicity is observed in NaCrGe and NaMnGe, which are suitable for spintronic applications. In contrast, both spin channels of NaFeGe and NaCoGe exhibit metallic nature since their electronic states overlap with the Fermi level. Large magnetic moments are produced by the spin-up 3d orbitals of V, Cr, Mn, and Fe, whereas low magnetism in NaCoGe is induced by the spin-down Co-3d state. All ten ternary compounds are mechanically stable, however their resistance, anisotropy, and ductile and brittle properties show a strong dependence on the TM chemical nature. Our results have clearly classified the effects of TM modification on the fundamental properties of NaTMGe compounds, which can be generalized to be useful information for future experimental and theoretical work dealing with Heusler materials containing 3d transition metals.

Conflicts of interest

The authors declare that they have no known competing financial interests or personal relationships that could have appeared to influence the work reported in this paper.

Acknowledgements

Tuan V. Vu would like to thank the Van Lang University for financial support.

Notes and references

1 P. Tedrow and R. Meservey, *Phys. Rev. B: Solid State*, 1973, **7**, 318.
2 M. Julliere, *Phys. Lett. A*, 1975, **54**, 225–226.
3 M. N. Baibich, J. M. Broto, A. Fert, F. N. Van Dau, F. Petroff, P. Etienne, G. Creuzet, A. Friederich and J. Chazelas, *Phys. Rev. Lett.*, 1988, **61**, 2472.
4 A. Hirohata, K. Yamada, Y. Nakatani, I.-L. Prejbeanu, B. Diény, P. Pirro and B. Hillebrands, *J. Magn. Magn. Mater.*, 2020, **509**, 166711.
5 S. Wolf, D. Awschalom, R. Buhrman, J. Daughton, V. S. von Molnár, M. Roukes, A. Y. Chtchelkanova and D. Treger, *Science*, 2001, **294**, 1488–1495.
6 V. K. Joshi, *Eng. Sci. Technol. an Int.*, 2016, **19**, 1503–1513.
7 B. T. Jonker, G. Kioseoglou, A. T. Hanbicki, C. H. Li and P. E. Thompson, *Nat. Phys.*, 2007, **3**, 542–546.
8 K. D. Belashchenko, J. K. Glasbrenner and A. L. Wysocki, *Phys. Rev. B: Condens. Matter Mater. Phys.*, 2012, **86**, 224402.
9 C. Gould, G. Schmidt, G. Richter, R. Fiederling, P. Grabs and L. Molenkamp, *Appl. Surf. Sci.*, 2002, **190**, 395–402.

10 J. S. Moodera, T. S. Santos and T. Nagahama, *J. Phys.: Condens. Matter*, 2007, **19**, 165202.
11 P. LeClair, J. Ha, H. Swagten, J. Kohlhepp, C. Van de Vin and W. De Jonge, *Appl. Phys. Lett.*, 2002, **80**, 625–627.
12 F. Casper, T. Graf, S. Chadov, B. Balke and C. Felser, *Semicond. Sci. Technol.*, 2012, **27**, 063001.
13 D. Hoat, N. H. Giang, M. Naseri, R. Ponce-Pérez, J. Rivas-Silva and G. H. Cocoletzi, *Phys. Lett. A*, 2020, **384**, 126589.
14 A. O. Oliynyk, E. Antono, T. D. Sparks, L. Ghadbeigi, M. W. Gaultois, B. Meredig and A. Mar, *Chem. Mater.*, 2016, **28**, 7324–7331.
15 C. S. Birkel, W. G. Zeier, J. E. Douglas, B. R. Lettiere, C. E. Mills, G. Seward, A. Birkel, M. L. Snedaker, Y. Zhang, G. J. Snyder, *et al.*, *Chem. Mater.*, 2012, **24**, 2558–2565.
16 J. Ma, V. I. Hegde, K. Munira, Y. Xie, S. Keshavarz, D. T. Mildebrath, C. Wolverton, A. W. Ghosh and W. Butler, *Phys. Rev. B*, 2017, **95**, 024411.
17 D. Hoat, D.-Q. Hoang, N. T. Binh, M. Naseri, J. Rivas-Silva, A. Kartamyshev and G. H. Cocoletzi, *Mater. Chem. Phys.*, 2021, **257**, 123695.
18 L. Bainsla and K. Suresh, *Appl. Phys. Rev.*, 2016, **3**, 031101.
19 R. De Groot, F. Mueller, P. Van Engen and K. Buschow, *Phys. Rev. Lett.*, 1983, **50**, 2024.
20 J. Kübler, A. William and C. Sommers, *Phys. Rev. B: Condens. Matter Mater. Phys.*, 1983, **28**, 1745.
21 S. Skaftouros, K. Özdoğan, E. Şaşıoğlu and I. Galanakis, *Phys. Rev. B: Condens. Matter Mater. Phys.*, 2013, **87**, 024420.
22 H. C. Kandpal, G. H. Fecher and C. Felser, *J. Phys. D: Appl. Phys.*, 2007, **40**, 1507.
23 V. Alijani, J. Winterlik, G. H. Fecher, S. S. Naghavi and C. Felser, *Phys. Rev. B: Condens. Matter Mater. Phys.*, 2011, **83**, 184428.
24 G. Xu, E. Liu, Y. Du, G. Li, G. Liu, W. Wang and G. Wu, *Europhys. Lett.*, 2013, **102**, 17007.
25 S. Skaftouros, K. Özdoğan, E. Şaşıoğlu and I. Galanakis, *Appl. Phys. Lett.*, 2013, **102**, 022402.
26 D. Hoat, D.-Q. Hoang, M. Naseri, J. Rivas-Silva, A. Kartamyshev and G. H. Cocoletzi, *RSC Adv.*, 2020, **10**, 25609–25617.
27 Y. Wang, X. Zhang, B. Ding, Z. Hou, E. Liu, Z. Liu, X. Xi, H. Zhang, G. Wu and W. Wang, *Comput. Mater. Sci.*, 2018, **150**, 321–324.
28 C. Hordequin, J. Nozieres and J. Pierre, *J. Magn. Magn. Mater.*, 1998, **183**, 225–231.
29 Z. Wen, T. Kubota, T. Yamamoto and K. Takanashi, *Sci. Rep.*, 2015, **5**, 1–10.
30 P. Bach, C. Rüster, C. Gould, C. R. Becker, G. Schmidt and L. W. Molenkamp, *J. Cryst. Growth*, 2003, **251**, 323–326.
31 P. Bach, A. Bader, C. Rüster, C. Gould, C. Becker, G. Schmidt, L. Molenkamp, W. Weigand, C. Kumpf, E. Umbach, *et al.*, *Appl. Phys. Lett.*, 2003, **83**, 521–523.
32 S. Chibani, O. Arbouche, M. Zemouli, Y. Benallou, K. Amara, N. Chami, M. Ameri and M. El Keurti, *Comput. Condens. Matter*, 2018, **16**, e00312.
33 X. Wang, Z. Cheng and G. Liu, *Materials*, 2017, **10**, 1078.
34 M. Bennani, Z. Aziz, S. Terkhi, E. Elandaloussi, B. Bouadjemi, D. Chenine, M. Benidris, O. Youb and S. Bentata, *J. Supercond. Novel Magn.*, 2021, **34**, 211–225.
35 R. Meenakshi, R. Aram Senthil Srinivasan, A. Amudhavalli, R. Rajeswarapalanichamy and K. Iyakutti, *Phase Transitions*, 2021, **94**, 415–435.
36 A. Dey, R. Sharma, S. A. Dar and H. H. Raza, *J. Supercond. Novel Magn.*, 2021, **34**, 781–796.
37 R. Umamaheswari, M. Yogeswari and G. Kalpana, *J. Magn. Magn. Mater.*, 2014, **350**, 167–173.
38 X. Wang, Z. Cheng, J. Wang, X.-L. Wang and G. Liu, *J. Mater. Chem. C*, 2016, **4**, 7176–7192.
39 W. Feng, D. Xiao, Y. Zhang and Y. Yao, *Phys. Rev. B: Condens. Matter Mater. Phys.*, 2010, **82**, 235121.
40 Y. Ciftci, *J. Nanosci. Nanotechnol. Appl.*, 2021, **5**, 2.
41 S. Kacimi, H. Mehnane and A. Zaoui, *J. Alloys Compd.*, 2014, **587**, 451–458.
42 W. Kohn and L. J. Sham, *Phys. Rev.*, 1965, **140**, A1133.
43 K. Schwarz and P. Blaha, *Comput. Mater. Sci.*, 2003, **28**, 259–273.
44 H. J. Monkhorst and J. D. Pack, *Phys. Rev. B: Solid State*, 1976, **13**, 5188.
45 J. P. Perdew, K. Burke and M. Ernzerhof, *Phys. Rev. Lett.*, 1996, **77**, 3865.
46 A. Becke and E. Johnson, *J. Chem. Phys.*, 2006, **124**, 221101.
47 F. Tran, P. Blaha and K. Schwarz, *J. Phys.: Condens. Matter*, 2007, **19**, 196208.
48 F. Tran and P. Blaha, *Phys. Rev. Lett.*, 2009, **102**, 226401.
49 M. Jamal, S. J. Asadabadi, I. Ahmad and H. R. Aliabad, *Comput. Mater. Sci.*, 2014, **95**, 592–599.
50 R. Golesorkhtabar, P. Pavone, J. Spitaler, P. Puschnig and C. Draxl, *Comput. Phys. Commun.*, 2013, **184**, 1861–1873.
51 M. Rostami, M. Abedi, P. Amantorkaman and F. Kanjouri, *Vacuum*, 2020, **175**, 109278.
52 E. Şaşioglu, L. Sandratskii and P. Bruno, *J. Phys.: Condens. Matter*, 2005, **17**, 995.
53 D. N. A. Baker, M. S. Abu-Jafar, A. A. Mousa, R. T. Jaradat, K. F. Ilaiwi and R. Khenata, *Mater. Chem. Phys.*, 2020, **240**, 122122.
54 V. Alijani, S. Ouardi, G. H. Fecher, J. Winterlik, S. S. Naghavi, X. Kozina, G. Stryganyuk, C. Felser, E. Ikenaga, Y. Yamashita, *et al.*, *Phys. Rev. B: Condens. Matter Mater. Phys.*, 2011, **84**, 224416.
55 A. Gencer, O. Surucu, D. Usanmaz, R. Khenata, A. Candan and G. Surucu, *J. Alloys Compd.*, 2021, **883**, 160869.
56 E. G. Özdemir and Z. Merdan, *J. Alloys Compd.*, 2019, **807**, 151656.
57 A. Amudhavalli, R. Rajeswarapalanichamy and K. Iyakutti, *J. Alloys Compd.*, 2017, **708**, 1216–1233.
58 F. Birch, *J. Geophys. Res.: Solid Earth*, 1978, **83**, 1257–1268.
59 A. Togo and I. Tanaka, *Scr. Mater.*, 2015, **108**, 1–5.
60 T. T. Hoang, S. Rhim and S. Hong, *Phys. Rev. Mater.*, 2022, **6**, 055001.
61 M. Rostami, M. Abedi, P. Amantorkaman and F. Kanjouri, *Vacuum*, 2020, **175**, 109278.
62 I. Galanakis and P. Mavropoulos, *J. Phys.: Condens. Matter*, 2007, **19**, 315213.

63 V. V. On, D. K. Nguyen, D. Hoat, R. Ponce-Pérez, J. Rivas-Silva and G. H. Cocoletzi, *Int. J. Quantum Chem.*, 2021, **121**, e26445.
64 V. I. Anisimov, J. Zaanen and O. K. Andersen, *Phys. Rev. B: Condens. Matter Mater. Phys.*, 1991, **44**, 943.
65 S. E. A. Yousif and O. Yassin, *J. Alloys Compd.*, 2010, **506**, 456–460.
66 H. Moulkhalwa, Y. Zaoui, K. Obodo, A. Belkadi, L. Beldi and B. Bouhafs, *J. Supercond. Novel Magn.*, 2019, **32**, 635–649.
67 F. Mouhat and F.-X. Coudert, *Phys. Rev. B: Condens. Matter Mater. Phys.*, 2014, **90**, 224104.
68 Y. Liu, Y. Jiang, R. Zhou and J. Feng, *J. Alloys Compd.*, 2014, **582**, 500–504.
69 T. Rotonda, *IOP Conference Series: Earth and Environmental Science*, 2021, p. 012005.
70 R. Gaillac, P. Pullumbi and F.-X. Coudert, *J. Phys.: Condens. Matter*, 2016, **28**, 275201.
71 S. Sun, Y. Liu, H. Fu, X. Guo, S. Ma, J. Lin, G. Guo, Y. Lei and R. Wang, *Adv. Eng. Mater.*, 2018, **20**, 1800295.